Communication

Mixed Self-Assembled Amphiphilic Polymeric Nanoparticles for Intranasal Drug Delivery

Inbar Schlachet, Hen Moshe Halamish and Alejandro Sosnik[1,*]

[1] Laboratory of Pharmaceutical Nanomaterials Science, Department of Materials Science and Engineering, Technion-Israel Institute of Technology, Haifa, Israel

* Correspondence: Laboratory of Pharmaceutical Nanomaterials Science, De-Jur Bldg., Office 607, Department of Materials Science and Engineering, Technion-Israel Institute of Technology, 3200003 Haifa, Israel; Email: sosnik@technion.ac.il, alesosnik@gmail.com; Tel.: +972-77-887-1971

Received: date; Accepted: date; Published: date

Abstract: Intranasal (i.n.) administration became an alternative strategy to bypass the blood-brain barrier and improve drug bioavailability in the brain. The main goal of this work was to preliminarily study the biodistribution of mixed amphiphilic mucoadhesive nanoparticles made of chitosan-*g*-poly(methyl methacrylate) and poly(vinyl alcohol)-*g*-poly(methyl methacrylate) and ionotropically crosslinked with sodium tripolyphosphate in the brain after intravenous (i.v.) and i.n. administration to Hsd:ICR mice. After i.v. administration, the highest nanoparticle accumulation was detected in the liver, among other peripheral organs. After i.n. administration of a 10-times smaller nanoparticle dose, the accumulation of the nanoparticles in off-target organs was much lower than after i.v. injection. In particular, the accumulation of the nanoparticles in the liver was 20 times lower than by i.v. When brains were analyzed separately, intravenously administered nanoparticles accumulated mainly in the "top" brain, reaching a maximum after 1h. Conversely, in i.n. administration, nanoparticles were detected in the "bottom" brain and the head (maximum reached after 2 h) owing to their retention in the nasal mucosa and could serve as a reservoir from which the drug is released and transported to the brain over time. Overall results indicate that i.n. nanoparticles reach similar brain bioavailability, though with a 10-fold smaller dose, and accumulate in off-target organs to a more limited extent and only after redistribution through the systemic circulation. At the same time, both administration routes seem to lead to differential accumulation in brain regions and thus, they could be beneficial in the treatment of different medical conditions.

Keywords: Central nervous system (CNS); blood-brain barrier (BBB); self-assembled polymeric nanoparticles; intranasal delivery; biodistribution

1. Introduction

The treatment of diseases of the central nervous system (CNS) by systemic drug administration is challenging owing to the presence of the blood-brain barrier (BBB) and the blood-cerebrospinal fluid barrier (BCSFB) [1]. The BBB excludes more than 95% of the small-molecule and biological drugs from crossing into the brain [2,3]. In addition, the BBB displays different efflux transporters that transport substrate molecules (e.g., drugs) out of the brain endothelium, against a concentration gradient [4,5]. Drugs that do not comply with fundamental physicochemical characteristics such as high lipid solubility, low molecular weight and less than 8-10 H bonds with water cannot cross the BBB and their bioavailability and pharmacological efficacy diminished [2].

New delivery approaches that increase drug delivery to the CNS are under intense investigation [6]. The transient disruption of the BBB by osmotic shrinkage of the endothelial cells together with

the opening of BBB tight junctions by intracarotid arterial infusion of non-diffusive solutes such as mannitol is one of them [7]. A main drawback is that increased permeability might also enable the passage of plasma proteins and result in abnormal neuronal function [8]. Another strategy is the use of carrier-mediated transport systems that transport nutrients such as glucose and amino acids into the CNS [8]. Drugs with the proper molecular design that not always complies with the structure-activity relationship can be recognized by these influx transporters and show high permeability across the BBB [2,8,9]. Over the last decades, a plethora of nanotechnology strategies have been investigated to overcome the limited ability to deliver active molecules from the systemic circulation into the CNS [10-15]. For this, drug-loaded nanoparticles of different nature (e.g., lipid, polymeric) and size are surface-decorated with ligands that bind receptors overexpressed in the BBB and cross the BBB by transcytosis [16,17].

The existence of a nose-to-brain pathway that bypasses the BBB has been evidenced by the accumulation and harm caused by environmental nanoparticulate matter in the CNS [18-21]. With the emergence of nanomedicine, different types of pure drug nanocrystals and nanoparticles were designed and their CNS bioavailability following intranasal (i.n.) administration assessed [22-26]. We demonstrated that the i.n. administration of the antiretroviral efavirenz nanoencapsulated within polymeric micelles made of poly(ethylene oxide)-*b*-poly(propylene oxide) block copolymers significant increases of its bioavailability in the brain of rat with respect to the intravenous (i.v.) route [27]. However, often, these polymeric micelles show limited encapsulation capacity for many hydrophobic cargos and limited physical stability over time. Aiming to understand the cellular pathways involved in this transport, we investigated the interaction of different polymeric nanoparticles with primary olfactory sensory neurons, cortical neurons and microglia isolated from olfactory bulb, olfactory epithelium and cortex of newborn rats [28]. Our results strongly suggested the involvement of microglia (and not neurons) in the nose-to-brain transport of nanoparticulate matter. More recently, we designed mucoadhesive multimicellar amphiphilic nanoparticles made of chitosan (CS) and poly(vinyl alcohol) (PVA) that were hydrophobized with pendant poly(methyl methacrylate) (PMMA) blocks [29-31]. These amphiphilic nanoparticles display greater encapsulation capacity than conventional polymeric micelles made of diblock and triblock copolymers. Aiming to capitalize on these versatile nanocarriers in mucosal drug delivery in general and in nose-to-brain administration in particular, we produced mixed CS-*g*-PMMA:PVA-*g*-PMMA nanoparticles and demonstrated that they cross a model of nasal epithelium *in vitro* [32]. In this work, we preliminarily investigated the biodistribution of these mixed nanoparticles after i.n. administration to mice and compared it to the i.v. route.

2. Results and Discussion

2.1. Production and characterization of the nanoparticles

Mixed nanoparticles were produced by the solvent casting method that comprised co-dissolution of identical amounts of CS-PMMA30 (a graft copolymer of CS and PMMA containing 30% w/w of PMMA) and PVA-PMMA16 (a graft copolymer of PVA and PMMA containing 16% w/w of PMMA) in dimethyl sulfoxide, drying under vacuum and redispersion in water [32,33]. Self-assembly takes place once the critical aggregation concentration (CAC) is surpassed. The CAC of CS-PMMA30 and PVA-PMMA16 is in the 0.04-0.05% w/v range [29-31]. Since the self-assembly process is random, by utilizing this method, we anticipated the formation of mixed nanoparticles with very similar qualitative and quantitative composition. To physically stabilize the nanoparticle, CS domains were crosslinked by the formation of a polyelectrolyte complex with sodium tripolyphosphate (TPP). The size, size distribution and zeta-potential (Z-potential) of 0.1% w/v non-crosslinked and crosslinked mixed CS-PMMA30:PVA-PMMA16 (1:1) nanoparticles was analyzed by dynamic light scattering (DLS), at 25ºC. Non-crosslinked and crosslnked nanoparticles showed monomodal size distribution (one size population), while the polydispersity index (PDI) which is a measure of the size distribution slightly changed with ionotropic crosslinking (**Figure 1a**); e.g., non-crosslinked mixed CS-

PMMA30:PVA-PMMA16 (1:1) nanoparticles showed a hydrodynamic diameter (D_h) of 193 ± 62 nm and a PDI of 0.23. This size is similar to the shown by pure CS-PMM30 (D_h of 184 ± 4 nm; PDI of 0.20) and larger than that of pure PVA-PMMA16 counterparts of the same concentration (D_h of 92 ± 4 nm and PDI of 0.14) [29-31]. Crosslinking of a 0.1% w/v nanoparticle suspension with TPP solution in water (1% w/v; 2.5 μL per mL of nanoparticles) resulted in an increase of the size to 249 ± 26 nm and of the PDI to 0.26. Pure crosslinked CS-PMM30 nanoparticles are larger 332 ± 54 nm (PDI of 0.33) owing to nanoparticle bridging, a phenomenon that is less likely in mixed particles that contain 50% w/w of non-ionic PVA-PPMA16, a copolymer that does not interact with TPP. The surface charge of nanoparticulate matter affects their cell compatibility and usually, positively-charged particles are more cytotoxic than neutral and negatively-charged ones [34]. Crosslinked nanoparticles (0.1% w/v) were also characterized by nanoparticle tracking analysis (NTA); the size being 142 ± 8 nm and the concentration 541 ± 27 x 10^9 particles/mL. NTA also allowed to visualize the Brownian motion of the nanoparticles in suspension (**Supplementary Video**).

CS is a biocompatible polysaccharide though it may elicit cell toxicity when it is not crosslinked [35]. Crosslinking of self-assembled CS-based nanoparticles was implemented to physically stabilize them and also to partly neutralize the net positive surface charge [36]; the zeta-potential of CS-PMMA30 nanoparticles decreased from +39 to +28 mV upon crosslinking. However, this modification was not enough to ensure good primary cell compatibility [36]. Thus, we produced mixed nanoparticles that reduce the effective CS concentration on the surface and thus, its charge density, while preserving the nanoencapsulation capacity of the nanoparticles and its mucoadhesiveness [32]. Further crosslinking reduced the Z-potential to +10 mV and improved the compatibility of the nanoparticles in primary nasal epithelial cells [32]. We confirmed the almost spherical morphology of non-crosslinked and crosslinked nanoparticles by high resolution-scanning electron microscopy (HR-SEM). In addition, the size was in good agreement with DLS analysis, considering that in HR-SEM the nanoparticles underwent drying (**Figure 1b,c**).

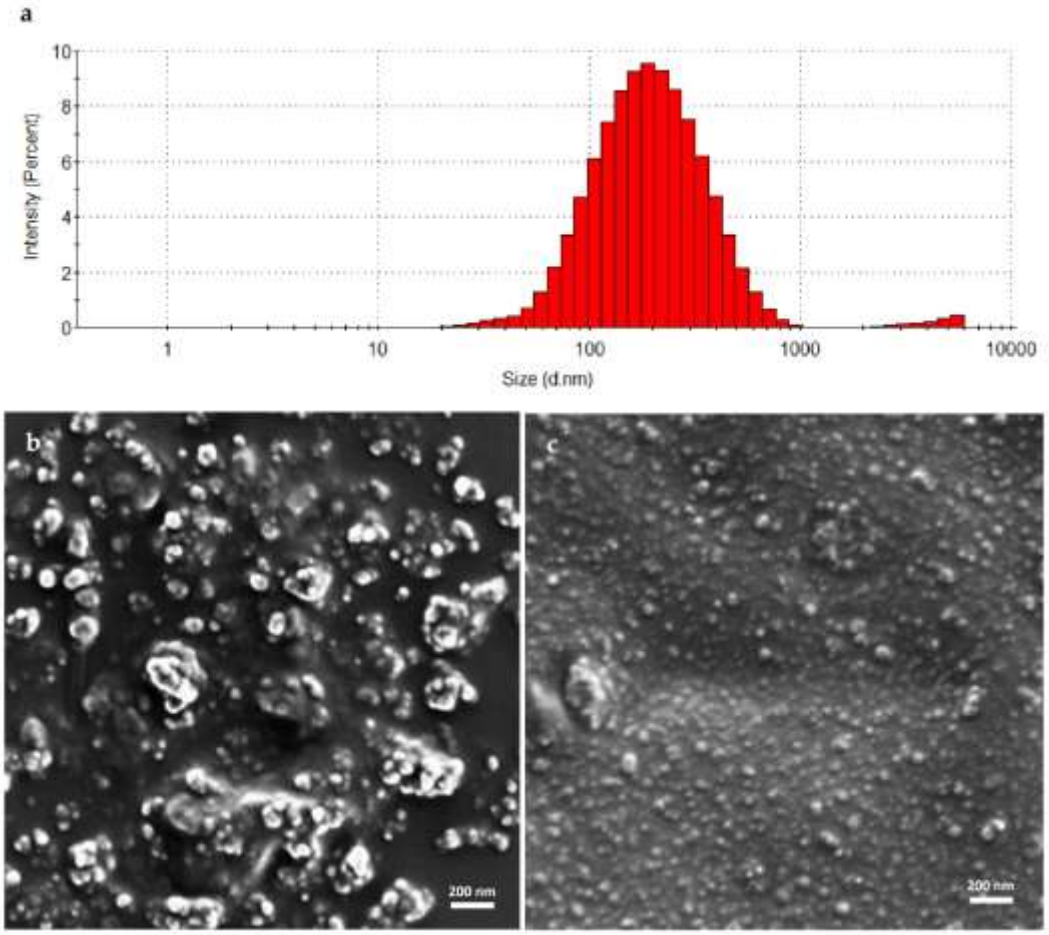

Figure 1. Characterization of mixed CS-*g*-PMMA:PVA-*g*-PMMA (1:1) nanoparticles. (a) Size distribution of crosslinked nanoparticles, as determined by DLS. (b,c) HR-SEM micrographs of (b) non-crosslinked and (c) crosslinked nanoparticles.

The stage of the work was focused on the investigation of the biodistribution of the mixed nanoparticles after i.n. and i.v. administration and their accumulation in the brain and other organs in Hsd:ICR mice. Since crosslinked nanoparticles display greater physical stability, for this, 0.1% w/v crosslinked mixed CS-PMMA30:PVA-PMMA16 (1:1) nanoparticles were labeled with the near infrared (NIR) dye NIR-797 and 200 μL of the nanoparticle suspension was injected i.v. through the tail vein or 20 μL of the same formulation was administered i.n. It is important to highlight that the i.n. nanoparticle dose in this preliminary study was 10-fold smaller than i.v.

At predetermined time points, live animal screening was performed using IVIS Spectrum In Vivo Imaging System. After i.v. administration, nanoparticles reach the systemic circulation and interact with the reticuloendothelial system, a system of macrophages mostly in the liver that could sequester the nanoparticles due the recognition of opsonins (serum proteins), while nanoparticles with size of up to 5-10 nm could undergo renal filtration [37]. At different time points post-administration, mice were sacrificed, the different organs dissected and the fluorescence radiance efficiency of each organ was measured and expressed as an average radiance with subtracting the basal signal of each organ in control (untreated) animals (**Figure 2**). After i.v. administration, the highest accumulation at the different time points was observed in the liver (**Figure 2a**), as described for other nanoparticles of similar size [37-39]. Other organs showed lower relative fluorescence associated with more limited nanoparticle accumulation, except for the kidneys. According to the size of the particles used in this work (several hundreds of nanometers), we did not expect to find nanoparticles in the kidneys. However, there are other particle parameters (e.g., charge) that affect their accumulation in this excretion organ. The i.n. is a local administration route that capitalizes on the nose-to-brain transport

to surpass the BBB and target the brain. Thus, accumulation in the different peripheral organs was not expected [40]. After i.n. administration, the accumulation of the nanoparticles in off-target organs was much lower than after i.v. injection (**Figure 2b**). In particular, the accumulation of the nanoparticles in the liver was 20 times lower than by i.v.; intranasally administered nanoparticles could reach peripheral organs after redistribution from the CNS to the systemic circulation [41,42].

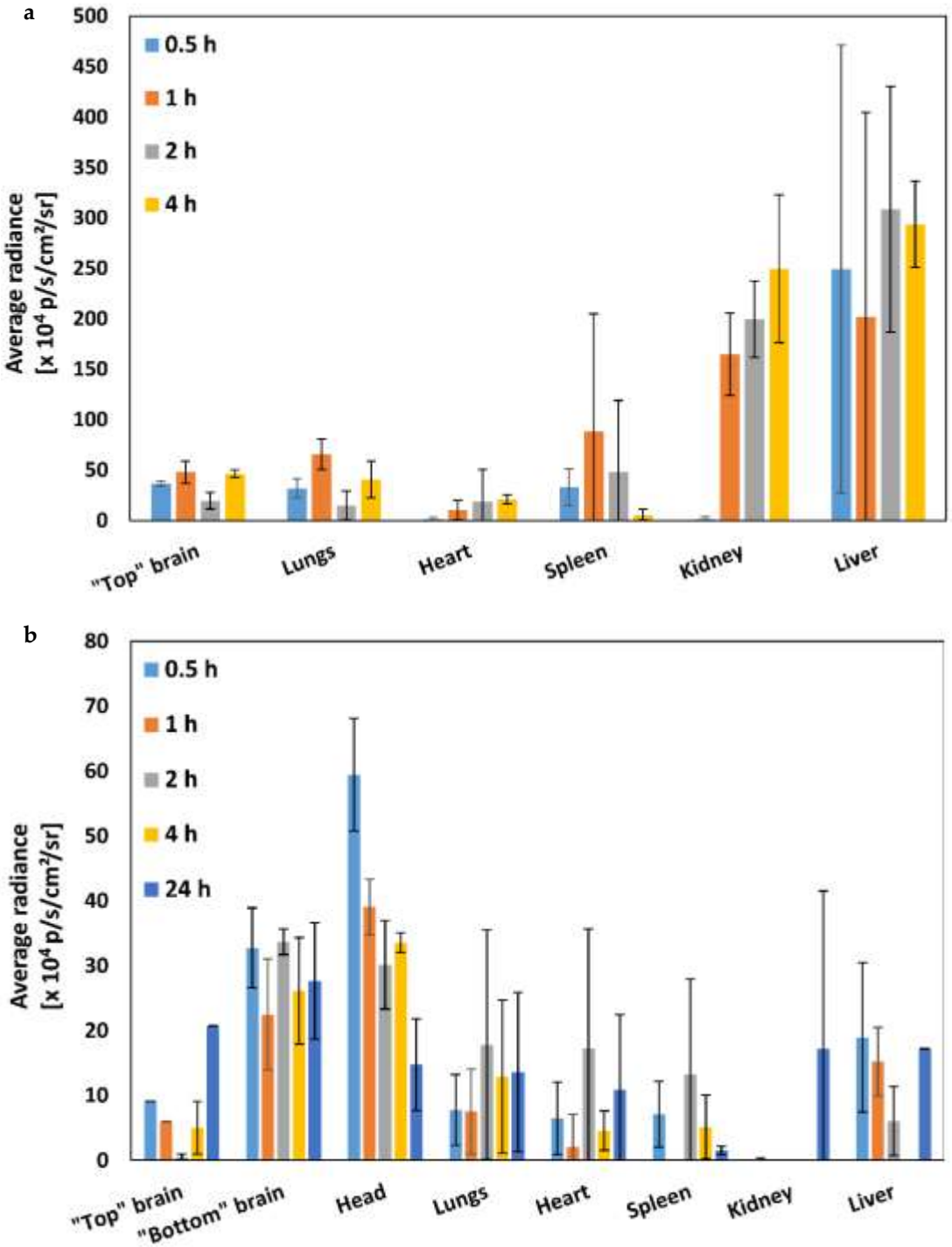

Figure 2. Biodistribution of NIR-797-labelled crosslinked 0.1% w/v mixed CS-PMMA30:PVA-PMMA16 nanoparticles (1:1) after (a) i.v. administration and (b) i.n. administration to Hsd:ICR mice (n = 3). The measurement was performed after organ dissection at each time point. Average radiance was measured using Living Imaging analysis software. Bars represent the average of mice at each time point. The error bars are S.D. from the mean.

The imaging system used in this study normalizes the average radiance to the organ displaying the maximum intensity. Thus, we imaged the brains separately from the other organs (in triplicates) at different time points and quantified the nanoparticle accumulation in the "top" and "bottom" brain after both administration routes (**Figure 3a**). Upon i.v. administration, nanoparticles accumulated mainly in the "top" brain. However, their ability to cross the BBB without surface modification with a ligand is limited [43]. Conversely, in the case of i.n. administration, particles are expected to access it through the olfactory region and accumulate in the nose, the nose-to-brain track (e.g., olfactory bulb) and the "bottom" brain (**Figure 3a**) [21,44].

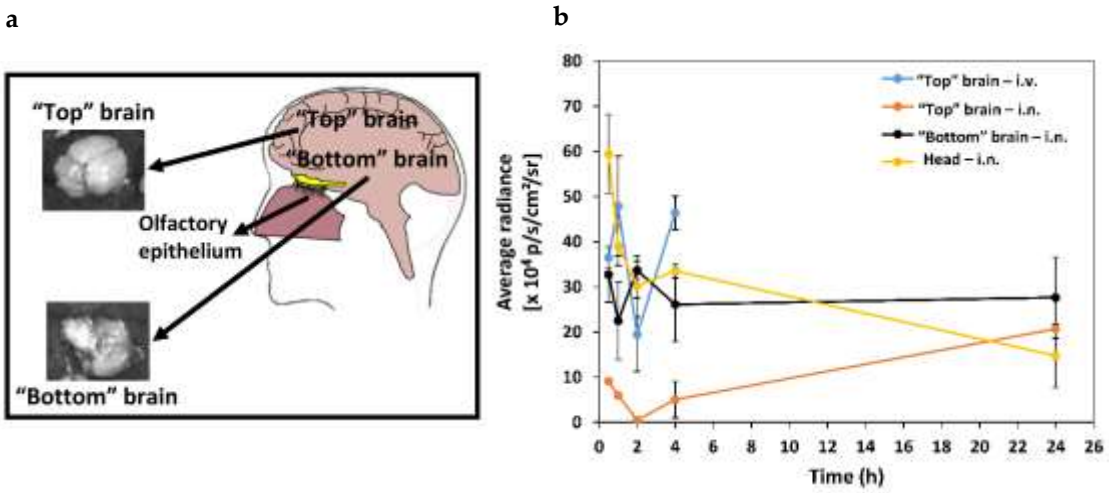

Figure 3. *Ex vivo* analysis of the distribution of NIR-797-labeled crosslinked 0.1% w/v mixed CS-PMMA30:PVA-PMMA16 nanoparticles (1:1) in the brain following i.v. and i.n. administration to Hsd:ICR mice (n = 3). (a) Scheme of the top and bottom brain and (b) average radiance over time obtained after the subtraction of the control (untreated mice brain) radiance (n = 3).

The highest accumulation was observed in the "top" brain 1 h after i.v. injection (**Figure 3b**). At this point, we analyzed the bottom side of the brain after i.n. administration because the nanoparticles could be accumulated in this area of the CNS close to the pons after penetrating through the olfactory epithelium and serve as a reservoir from which an encapsulated drug could be released. Two hours after i.n. administration, the accumulation in the "bottom" brain was significantly higher than upon i.v. injection. We further calculated the average radiance in the brain (with subtraction of the control signal) at each time point and compared values of area under the curve (AUC) between 0 and 4 h ($AUC_{0\text{-}4\ h}$). Nanoparticle accumulation in the "bottom" brain after i.n. administration ($AUC_{0\text{-}4\ h}$ = 110 ± 10 x 10^4 p/s/cm²/sr) was similar and not significantly different from that of intravenously administered nanoparticles in the "top" brain ($AUC_{0\text{-}4\ h}$ = 130 ± 20 x 10^4 p/s/cm²/sr) (**Figure 3b, Table 1**). These results indicated that a similar brain bioavailability could be reached with a 10 times smaller dose. At the same time, both administration routes seem to lead to differential accumulation in brain regions and thus, they could be beneficial in the treatment of different medical conditions.

Table 1. Average radiance obtained from different brain regions and the head after the subtraction of the control (untreated mice) radiance at different time points and calculated $AUC_{0\text{-}4\,h}$ values.

Brain region	$AUC_{0\text{-}4\,h}$ (x 10^4 p/s/cm²/sr) ± S.D.
"Top brain" – i.v.	130 ± 20
"Top brain" – i.n.	15 ± 4
"Bottom brain" – i.n.	110 ± 18
Head – i.n.	138 ± 17

A remarkable advantage of i.n. administration is that the exposure of off-target organs to the nanoparticles and eventually the encapsulated drug is dramatically reduced. In addition, after i.n. administration, we analyzed the head including the skull to reveal whether these mucoadhesive nanoparticles are retained in the nasal cavity upon interaction with the nasal mucosa or not. Nanoparticles were detected in head and more specifically in the nose with an $AUC_{0\text{-}4\,h}$ of 138 ± 17 x 10^4 p/s/cm²/sr (**Table 1**). These findings indicated that a high fraction of the nanoparticles remains mucoadhered in the nose, and could serve as reservoir from which the drug is released and transported to the CNS. Next studies will investigate the pharmacokinetics of encapsulated drugs in the CNS upon i.v. and i.n. administration.

4. Methods

4.1. Synthesis of the chitosan-g-poly(methyl methacrylate) and poly(vinyl alcohol)-g-poly(methyl methacrylate) copolymers

A CS-*g*-PMMA copolymer containing 30% w/w of PMMA (CS-PMMA30, as determined by proton-nuclear magnetic resonance [29,30]), was synthesized by the graft free radical polymerization of MMA (99% purity, Alfa Aesar, Heysham, UK) onto the CS backbone in water. For this, low molecular weight CS (0.4 g, degree of deacetylation of 94%; viscosity ≤ 100 mPa.s, Glentham Life Sciences, Corsham, UK) was dissolved in nitric acid 70% (0.05 M in water, 100 mL) that was degassed by sonication (30 min, Elmasonic S 30, Elma Schmidbauer GmbH, Singen, Germany). Then, a tetramethylethylenediamine (TEMED, Alfa Aesar) solution (0.18 mL in 50 mL of degassed water) was poured into the CS solution and purged with nitrogen for 30 min at RT. The purged CS solution was magnetically stirred and heated to 35°C and 142 µL of MMA (distilled under vacuum to remove inhibitors before use) was added to the degassed water (48 mL) and then mixed with the CS solution. Finally, a cerium (IV) ammonium nitrate (CAN, Strem Chemicals, Inc., Newburyport, MA) solution (0.66 g in 2 mL of degassed water) was added to the polymerization reaction that was allowed to proceed for 3 h at 35°C and under continuous nitrogen flow. After 3 h, the polymerization was quenched by adding 0.13 g of hydroquinone (Merck, Hohenbrunn, Germany). The product was purified by dialysis against distilled water using a regenerated cellulose dialysis membrane with molecular weight-cut off (MWCO) of 12–14 kDa (Spectra/Por® 4 nominal flat width of 75 mm, diameter of 48 mm and volume/length ratio of 18 mL/cm, Spectrum Laboratories, Inc., Rancho Dominguez, CA, USA) for at 48–72 h and freeze-dried. The same chemical pathway with small modifications was used to synthesize a PVA-*g*-PMMA copolymer containing 16% w/w of PMMA (PVA-PMMA16) [31]. First, PVA (0.4 g) was dissolved in distilled water (100 mL) at RT and TEMED (0.18 mL in 50 mL of degassed water) was dissolved in nitric acid 70% (0.45 mL). Then, TEMED and PVA solutions were degassed by sonication for 30 min, mixed and purged with nitrogen for 30 min at RT. The solution was heated to 35°C and 142 µL of MMA dispersed in degassed water (48 mL) and added to the reaction mixture. Finally, a CAN solution (0.66 g in 2 mL of degassed water) was added and the reaction allowed to proceed for 2 h at 35°C. The reaction product was purified by dialysis and freeze-dried. Products were stored at 4°C until use.

For biodistribution studies (see below), CS-PMMA30 and PVA-PMMA16 copolymers were fluorescently-labeled with the near infrared tracer NIR-797 isocyanate (Sigma-Aldrich, St. Louis, MO, USA). For this, CS-PMMA30 (80 mg) was dissolved in 8 mL water supplemented with acetic acid (pH = 5.5), prepared by diluting 70 μL of glacial acetic acid (Bio-Lab Ltd., Jerusalem, Israel) in 1 L of water under magnetic stirring. Then, NIR-797 (0.4 mg) was dissolved in *N*,*N*-dimethylformamide (0.2 mL, DMF, Bio-Lab Ltd.), added to the copolymer solution and the mixture stirred for 16 h protected from light, at RT. Finally, the product was dialyzed (48 h, regenerated cellulose dialysis membrane, MWCO of 3500 Da, Membrane Filtration Products, Inc., Seguin, TX, USA), freeze-dried (72–96 h) and stored protected from light at 4ºC until use. In the case of PVA-PMMA16, the copolymer (100 mg) was dissolved in 3 mL DMF under magnetic stirring. Then, NIR-797 (0.8 mg) was dissolved in DMF (0.1 mL), added to the copolymer solution and the mixture stirred for 16 h protected from light, at RT. The reaction mixture was diluted with deionized water (1:2 v/v), dialyzed (48 h, regenerated cellulose dialysis membrane, MWCO of 3500 Da) to remove unreacted NIR-797, freeze-dried (72–96 h) and stored protected from light at 4ºC until use.

4.2. Preparation and characterization of mixed chitosan-g-poly(methyl methacrylate):poly(vinyl alcohol)-g-poly(methyl methacrylate) nanoparticles

Identical amounts of CS-PMMA30 and PVA-PMMA16 were dissolved in dimehtyl sulfoxide (DMSO) to reach a total copolymer concentration of 0.5% w/v under continuous stirring (24 h), at 37ºC. Subsequently, the solution was dried under vacuum utilizing a freeze-dryer, the copolymer mixture re-dispersed in water supplemented with acetic acid (pH = 5.5) to reach a final total copolymer concentration of 0.1% w/v and filtered (1.2 μm cellulose acetate syringe filter, Sartorius Stedim Biotech GmbH, Göttingen, Germany). For physical stabilization, 0.1% w/v nanoparticles were crosslinked by the addition of 1% w/v TPP (Sigma-Aldrich) aqueous solution (2.5 μL of crosslinking solution per mL of 0.1% w/v nanoparticle dispersion).

The size (expressed as hydrodynamic diameter, D_h), size distribution (polydispersity index, PDI) and the zeta-potential (Z-potential, an estimation of the surface charge density) of 0.1% w/v systems were measured using the Zetasizer Nano-ZS in the same media detailed above for the different samples. Z-potential measurements of the same samples required the use of laser Doppler micro-electrophoresis in the Zetasizer Nano-ZS. Each value obtained is expressed as mean ± standard deviation (S.D.) of at least three independent samples, while each DLS or Z-potential measurement is an average of at least seven runs.

To quantify the number of particles per volume unit (in mL) and visualize their Brownian motion in suspension, samples were analyzed by NTA (NanoSight® NS500-Zeta HSB system with high sensitivity camera and 638 nm laser for fluorescent analysis, Malvern Instruments, Malvern, UK) under scattering and fluorescent mode. Nanoparticles were diluted in the same medium used to prepare the sample to fit the measurement range of the instrument (10^7-10^9 particles/mL) and immediately measured. Experimental concentrations (particle per mL) were corrected by the dilution factor.

The morphology of mixed nanoparticles before and after crosslinking was visualized by HR-SEM (carbon coating, acceleration voltage of 2-4 kV, Ultraplus, Zeiss, Oberkochen, Germany). For this, mixed nanoparticle suspensions (0.5% w/v total copolymer concentration), drop-casted on silicon wafer, dried at 37 ºC in the oven and carbon-coated. Images were obtained using In-lens detector at 3-4 mm working distance. The nanosuspensions were sprayed on top of a silicon wafer (cz polished silicon wafers <100> oriented, highly doped N/Arsenic, SHE Europe Ltd., Livingston, UK) by introducing high pressure nitrogen which allowed an even spread of the nanoparticles on the wafer. Next, the wafer was attached to the grid using carbon-tape and additional tape was placed on its frame. At the corners of the frame silver paint (SPI# 05002-AB – Silver, SPI supplies, West Chester, PA, USA) was applied and the samples were carbon coated.

4.3. Biodistribution of mixed chitosan-g-poly(methyl methacrylate):poly(vinyl alcohol)-g-poly(methyl methacrylate) nanoparticles

Hsd:ICR mice (Envigo, Jerusalem, Israel) were maintained at the Gutwirth animal facility of the Technion-Israel Institute of Technology. All animal experiments were approved and performed according to the guidelines of the Institutional Animal Research Ethical Committee at the Technion (ethics approval number IL-052-05-18). Animal welfare was monitored daily by the staff veterinarians. Mice fasted for 12 h prior to experiments. Crosslinked mixed CS-PMMA30:PVA-PMMA16 (1:1) nanoparticles (200 µL, 0.1% w/v) were injected i.v. into the tail vein. For i.n. administration, mice were lightly anesthetized with 2.5% isoflurane (USP Terrel™ Piramal Critical Care, Bethlehem, PA, USA), and fixed in a supine position for the administration of 10 µL of the nanoparticles in each nostril using a pipette (total volume of 20 µL, 0.1% w/v). After 0.5, 1, 2, 4 and 24 h post i.v. injection or i.n. administration animals were sacrificed by dislocation and organs (liver, spleen, kidney, lungs, heart, brain and head – nose area) were dissected. Organ screening was performed *ex vivo* using an Imaging System (IVIS, PerkinElmer, Waltham, MA, USA) with an excitation at 795 nm and an emission at 810 nm. Then at the same conditions (see above) image analysis was performed using Living Imaging analysis software (PerkinElmer). The auto fluorescence of organs of the control (untreated) mouse were subtracted. Mice were used in triplicates for each time point. Then, the average radiance in the brain (with subtraction of the control signal) at each time point was calculated, and the values of $AUC_{0\text{-}4\ h}$ determined according to Equation 1 [45]

$$AUC = \sum_i \frac{(t_{i+1} - t_i)}{2 \times (AR_i + AR_{i+1})} \quad (1)$$

Where t_i is the starting time point, t_{i+1} is the finishing time point (0.5, 1, 2 and 4 h), AR_i is the starting value of average fluorescence measured, and AR_{i+1} is the finishing value for each measurement over time.

4.4. Statistical analysis

Statistical analysis of the different experiments was performed by t-test on raw data (Excel, Microsoft Office 2013, Microsoft Corporation). P-values of less than 0.05 were regarded as statistically significant.

Supplementary Materials: The following are available online at www.mdpi.com/xxx/s1
Supplementary video: Brownian motion of mixed crosslinked CS-PMMA30:PVA-PMMA16 (1:1) nanoparticles.

Funding: This work was supported by the Israel Science Foundation (ISF, Grant #269/15) and the Teva National Network of Excellence in Neuroscience Research Grant. Partial support of the Russell Berrie Nanotechnology Institute (Technion) is also acknowledged.

Conflicts of Interest: The authors declare no conflict of interest

References

1. Blanco-Prieto, M. Drug Delivery to the Central Nervous System: A Review. *J. Pharm. Sci.* **2003**, *6*, 252–273.
2. Pardridge, W. Non-Invasive Drug Delivery to the Human Brain Using Endogenous Blood-Brain Barrier Transport Systems. *Pharm. Sci. Technol. Today.* **1999**, *2*, 49–59.
3. Oller-Salvia, B.; Sanchez-Navarro, M.; Giralt, E.; Teixido, M. Blood-Brain Barrier Shuttle Peptides: An Emerging Paradigm for Brain Delivery. *Chem. Soc. Rev.* **2016**, *45* (17), 4690–4707.
4. Löscher, W., Potschka, H. Blood-Brain Barrier Active Efflux Transporters: ATP-Binding Cassette Gene Family. *NeuroRx* **2005**, *2*, 86–98.

5. Dallas, S.; Miller, D.S.; Bendayan, R. Multidrug Resistance-Associated Proteins: Expression and Function in the Central Nervous System. *Pharmacol. Rev.* **2006**, *58*, 140–161.
6. Zeiadeh, I.; Najjar, A.; Karaman, R. Strategies for Enhancing the Permeation of CNS-Active Drugs through the Blood-Brain Barrier: A Review. *Molecules* **2018**, *23*, 1289.
7. Rapoport, S.I. Osmotic Opening of the Blood–Brain Barrier: Principles, Mechanism, and Therapeutic Applications. *Cell Mol. Neurobiol.* **2000**, *20*, 217–230.
8. Ohtsuki, S., Terasaki, T. Contribution of Carrier-Mediated Transport Systems to the Blood–Brain Barrier as a Supporting and Protecting Interface for the Brain; Importance for CNS Drug Discovery and Development. *Pharm. Res.* **2007**, *24*, 1745–1758.
9. Tsuji, A. Small Molecular Drug Transfer Across the Blood-Brain Barrier via Carrier-Mediated Transport Systems. *NeuroRx* **2005**, *2*, 54–62.
10. Gomes M.J., Mendes B., Martins S., Sarmento B. (2016) Nanoparticle Functionalization for Brain Targeting Drug Delivery and Diagnostic. In: Aliofkhazraei M. (eds) Handbook of Nanoparticles. Springer, Cham.
11. Gabathuler, R. Approaches to Transport Therapeutic Drugs Across the Blood-Brain Barrier to Treat Brain Diseases. *Neurobiol. Dis.* **2010**, *37*, 48–57.
12. Fang, F.; Zou, D.; Wang, W.; Yin, Y.; Yin, T.; Hao, S.; Wang, B.; Wang, G.; Wang, Y. Non-Invasive Approaches for Drug Delivery to the Brain Based on the Receptor Mediated Transport. *Mater. Sci. Eng. C* **2017**, *76*, 1316–1327.
13. Tam, V.H.; Sosa, C.; Liu, R.; Yao, N.; Priestley, R.D.; Nanomedicine as a Non-Invasive Strategy for Drug Delivery Across the Blood Brain Barrier. *Int. J. Pharm.* **2016**, *515*, 331–342.
14. Gaillard, P.J.; Visser, C. C.; Appeldoorn, C.C.M.; Rip, J. Enhanced Brain Drug Delivery: Safely Crossing the Blood-Brain Barrier. *Drug Discov. Today Technol.* **2012**, *9*, 155–160.
15. Wong, H.L.; Wu, X.Y.; Bendayan, R. Nanotechnological Advances for the Delivery of CNS Therapeutics. *Adv. Drug Deliv. Rev.* **2012**, *64*, 686–700.
16. Saraiva, C.; Praca, C.; Ferreira, R.; Santos, T.; Ferreira, L.; Bernardino, L. Nanoparticle-Mediated Brain Drug Delivery: Overcoming Blood-Brain Barrier to Treat Neurodegenerative Diseases. *J. Control. Release.* **2016**, *235*, 34–47.
17. Georgieva, J. V.; Hoekstra, D.; Zuhorn, I. S. Smuggling Drugs into the Brain: An Overview of Ligands Targeting Transcytosis for Drug Delivery across the Blood Brain Barrier. *Pharmaceutics.* **2014**, *6*, 557–583
18. Lucchini, R.G.; Dorman, D.C.; Elder, A.; Veronesi, B. Neurological Impacts from Inhalation of Pollutants and the Nose-Brain Connection. *Neurotoxicology* **2012,** *33*, 838-841.
19. Oberdörster, G.; Sharp, Z.; Atudorei, V.; Elder, A.; Gelein, R.; Kreyling, W.; Cox, C. Translocation of Inhaled Ultrafine Particles to the Brain. *Inhal. Toxicol.* **2004,** *16*, 437-445.
20. Elder, A.; Gelein, R.; Silva, V.; Feikert, T.; Opanashuk, L.; Carter, J.; Potter, R.; Maynard, A.; Ito, Y.; Finkelstein, J.; Oberdörster, G. Translocation of Inhaled Ultrafine Manganese Oxide Particles to the Central Nervous System. *Environ. Health. Perspect.* **2006,** *114*, 1172.
21. Babadjouni, R.; Patel, A.; Liu, Q.; Shkirkova, K.; Lamorie-Foote, K.; Connor, M.; Hodis, D.M.; Cheng, H.; Sioutas, C.; Morgan, T.E.; Finch, C.E.; Mack, W.J. Nanoparticulate Matter Exposure Results in Neuroinflammatory Changes in the Corpus Callosum. *PLOS One* **2018,** *13*, e0206934.

22. Pires, P.C.; Santos, A.O. Nanosystems in Nose-To-Brain Drug Delivery: A Review of Non-Clinical Brain Targeting Studies. *J. Control. Release* **2018,** *270*, 89-100.
23. Feng, Y.; He, H.; Li, F.; Lu, Y.; Qi, J.; Wu, W. An Update on the Role of Nanovehicles in Nose-to-Brain Drug Delivery. *Drug Discov. Today* **2018**, *23*, 1079-1088.
24. Hanson, L.R.; Frey, W.H. Intranasal Delivery Bypasses the Blood-Brain Barrier to Target Therapeutic Agents to the Central Nervous System and Treat Neurodegenerative Disease. *BMC Neurosci.* **2008,** *9*, S5.
25. Perez, A.P.; Mundiña-Weilenmann, C.; Romero, E.L.; Morilla, M.J. Increased Brain Radioactivity by Intranasal P-labeled siRNA Dendriplexes Within in Situ-Forming Mucoadhesive Gels. *Int. J. Nanomedicine* **2012,** *7*, 1373-1385.
26. Kumar, A.; Pandey, A.N.; Jain, S.K. Nasal-Nanotechnology: Revolution for Efficient Therapeutics Delivery. *Drug Deliv.* **2016**, *23*, 671-683.
27. Chiappetta, D.A.; Hocht, C.; Opezzo, J.A.W.; Sosnik, A, Intranasal Administration of Antiretroviral-Loaded Micelles for Anatomical Targeting to the Brain in HIV. *Nanomedicine (Lond.)* **2013**, *8*, 223-237.
28. Kumarasamy, M.; Sosnik, A. The Nose-to-Brain Transport of Polymeric Nanoparticles is Mediated by Immune Sentinels and Not by Olfactory Sensory Neurons. *Adv. Biosys.* **2019**, *3*, 1900123.
29. Noi, I.; Schlachet, I.; Kumarasamy, M.; **Sosnik, A.** Permeability of Chitosan-*g*-Poly(Methyl Methacrylate) Amphiphilic Nanoparticles in a Model of Small Intestine *In Vitro*. *Polymers* **2018**, *10*, 478.
30. Schlachet, I.; Trousil, J.; Rak, D.; Knudsen, K.D.; Pavlova, E.; Nyström, B.; Sosnik, A. Chitosan-*graft*-Poly(Methyl Methacrylate) Amphiphilic Nanoparticles: Self-Association and Physicochemical Characterization. *Carbohydr. Polym.* **2019**, *212*, 412-420.
31. Moshe Halamish, H.; Trousil, J.; Rak, D.; Knudsen, K.D.; Pavlova, E.; Nyström, B.; Štěpánek, P.; Sosnik, A. Self-Assembly and Nanostructure of Poly(Vinyl Alcohol)-*graft*-Poly(Methyl Methacrylate) Amphiphilic Nanoparticles. *J. Colloid Interface Sci.* **2019**, *553*, 512-523.
32. Schlachet, I.; Sosnik, A. Mixed Mucoadhesive Amphiphilic Polymeric Nanoparticles Cross a Model of Nasal Septum Epithelium In Vitro. *ACS Appl. Mater. Interfaces* **2019**, *11*, 21360–21371.
33. Gaucher, G.; Dufresne, M.-H.; Sant, V. P.; Kang, N.; Maysinger, D.; Leroux, J.-C. Block Copolymer Micelles: Preparation, Characterization and Application in Drug Delivery. *J. Control. Release.* **2005**, *109*, 169–188.
34. Fröhlich, E. The Role of Surface Charge in Cellular Uptake and Cytotoxicity of Medical Nanoparticles. *Int. J. Nanomedicine* **2012**, *7*, 5577–5591.
35. Rizeq, B.R.; Younes, N.N.; Rasool, K.; Nasrallah, G.K. Synthesis, Bioapplications, and Toxicity Evaluation of Chitosan-Based Nanoparticles. *Int. J. Mol. Sci.* **2019**, *20*, 5776.
36. Raskin Menaker, M.; Schlachet, I.; Sosnik, A. Mucoadhesive Nanogels by Ionotropic Crosslinking of Chitosan-*g*-Oligo(NiPAam) Polymeric Micelles as Novel Drug Nanocarriers. *Nanomedicine (Lond.).* **2016**, *11*, 217–233.
37. Ernsting, M. J.; Murakami, M.; Roy, A.; Li, S. D. Factors Controlling the Pharmacokinetics, Biodistribution and Intratumoral Penetration of Nanoparticles. *J. Control. Release* **2013**, *172*, 782–794.
38. He, C.; Hu, Y.; Yin, L.; Tang, C.; Yin, C. Effects of Particle Size and Surface Charge on Cellular Uptake and Biodistribution of Polymeric Nanoparticles. *Biomaterials* **2010**, *31*, 3657–3666.
39. Hirn, S.; Semmler-Behnke, M.; Schleh, C.; Wenk, A.; Lipka, J.; Schäffler, M.; Takenaka, S.; Möller, W.; Schmid, G.; Simon, U.; et al. Particle Size-Dependent and Surface Charge-Dependent Biodistribution of Gold Nanoparticles after Intravenous Administration. *Eur. J. Pharm. Biopharm.* **2011**, *77*, 407–416.

40. Yadav, S.; Gattacceca, F.; Panicucci, R.; Amiji, M. M. Comparative Biodistribution and Pharmacokinetic Analysis of Cyclosporine-A in the Brain upon Intranasal or Intravenous Administration in an Oil-in-Water Nanoemulsion Formulation. *Mol. Pharmaceutics* **2015**, *12*, 1523–1533.

41. Gao, X.; Chen, J.; Chen J.; Wu, B.; Chen, H.; Jiang, X. Quantum Dots Bearing Lectin-Functionalized Nanoparticles as a Platform for In Vivo Brain Imaging. *Bioconjug. Chem.* **2008**, *19*, 2189-2195.

42. Sekerdag. E.; Lüle, S.; Bozdağ Pehlivan, S.; Öztürk, N.; Kara, A.; Kaffashi, A.; Vural, I.; Işıkay, I.; Yavuz, B.; Oguz, K.K.; Söylemezoğlu, F.; Gürsoy-Özdemir, Y.; Mut, M. A Potential Non-Invasive Glioblastoma Treatment: Nose-to-Brain Delivery of Farnesylthiosalicylic Acid Incorporated Hybrid Nanoparticles. *J. Control. Release* **2017**, 261, 187-198.

43. Bukchin, A.; Sanchez-Navarro, M.; Carrera, A.; Teixidó, M.; Carcaboso, A.M.; Giralt, E.; Sosnik, A. Amphiphilic Polymeric Nanoparticles Modified with a Retro-Enantio Peptide Shuttle Target the Brain of Mice**,** submitted.

44. Shiga, H.; Taki, J.; Yamada, M.; Washiyama, K.; Amano, R.; Matsuura, Y.; Matsui, O.; Tatsutomi, S.; Yagi, S.; Tsuchida, A.; Yoshizaki, T.; Furukawa, M.; Kinuya, S.; Miwa, T. Evaluation of the Olfactory Nerve Transport Function by SPECT-MRI Fusion Image with Nasal Thallium-201 Administration. *Mol. Imaging Biol.* **2011**, *13*, 1262-1266.

45. Pardi, N.; Hogan, M. J.; Naradikian, M. S.; Parkhouse, K.; Cain, D. W.; Jones, L.; Moody, M. A.; Verkerke, H. P.; Myles, A.; Willis, E.; LaBranche, C.C.; Montefiori, D.C.; Lobby, J.L.; Saunders, K.O.; Liao, H.X.; Korber, B.T.; Sutherland, L.L.; Scearce, R.M.; Hraber, P.T.; Tombácz, I.; Muramatsu, H.; Ni, H.; Balikov, D.A.; Li, C.; Mui, B.L.; Tam, Y.K.; Krammer, F.; Karikó, K.; Polacino, P.; Eisenlohr, L.C.; Madden, T.D.; Hope, M.J.; Lewis, M.G.; Lee, K.K.; Hu, S.L.; Hensley, S.E.; Cancro, M.P.; Haynes, B.F.; Weissman, D. Nucleoside-Modified MRNA Vaccines Induce Potent T Follicular Helper and Germinal Center B Cell Responses. *J. Exp. Med*. **2018**, *215*, 1571–1588.